Effect of Molecular Weight on the Structure and Crystallinity of Poly(3-hexylthiophene)

Achmad Zen,[†] Marina Saphiannikova,[†,ϕ] Dieter Neher,*[,†] Jörg Grenzer,[‡] Souren Grigorian,[†,#] Ullrich Pietsch,[†,#] Udom Asawapirom,[⊥] Silvia Janietz,[⊥] Ullrich Scherf,[||] Ingo Lieberwirth,[§] and Gerhard Wegner[§]

Institute of Physics, University of Potsdam, Am Neuen Palais 10, D-14469 Potsdam, Germany; Institute of Ion Beam Physics and Materials Research, Bautzner Landstrasse 128, D-01328 Dresden, Germany; Fraunhofer Institute for Applied Polymer Research, Geiselberg-Str. 69, D-14476 Golm, Germany; Macromolecular Chemistry, University of Wuppertal, Gauss-Str. 20, D-42097 Wuppertal, Germany; and Max Planck Institute for Polymer Research, Ackermannweg 10, D-55128 Mainz, Germany

Received October 2, 2005; Revised Manuscript Received January 7, 2006

ABSTRACT: Recently, two different groups have reported independently that the mobility of field-effect transistors made from regioregular poly(3-hexylthiophene) (P3HT) increases strongly with molecular weight. Two different models were presented: one proposing carrier trapping at grain boundaries and the second putting emphasis on the conformation and packing of the polymer chains in the thin layers for different molecular weights. Here, we present the results of detailed investigations of powders and thin films of deuterated P3HT fractions with different molecular weight. For powder samples, gel permeation chromatography (GPC), differential scanning calorimetry (DSC), and X-ray diffraction (XRD) were used to investigate the structure and crystallization behavior of the polymers. The GPC investigations show that all weight fractions possess a rather broad molecular weight distribution. DSC measurements reveal a strong decrease of the crystallization temperature and, most important, a significant decrease of the degree of crystallinity with decreasing molecular weight. To study the structure of thin layers in lateral and vertical directions, both transmission electron microscopy (TEM) and X-ray grazing incidence diffraction (GID) were utilized. These methods show that thin layers of the low molecular weight fraction consist of well-defined crystalline domains embedded in a disordered matrix. We propose that the transport properties of layers prepared from fractions of poly(3-hexylthiophene) with different molecular weight are largely determined by the crystallinity of the samples and not by the perfection of the packing of the chains in the individual crystallites.

I. Introduction

Poly(hexylthiophene) (PHT) is one of the most studied polymers for organic field-effect transistor (OFET) applications.[1] This is mainly due to the fact that PHT provides excellent electrical properties while the presence of the hexyl substituents makes PHT well soluble and processable. The first demonstration to the usage of solution-processable polythiophene for OFET application was with regiorandom PHT.[2] In this case, the thin films were cast from chloroform and exhibited mobilities in the range of $10^{-5}-10^{-4}$ cm^2 V^{-1} s^{-1}. It was shown later that the charge-transporting properties of PHT depended strongly on whether the polymer is regiorandom or regioregular.[3] In fact, OFETs exhibiting mobilities of up to 0.045 and then 0.1 cm^2 V^{-1} s^{-1} have been prepared from highly regioregular P3HT.[3,4] These high values were explained by the ability of the polymer to adopt a well-ordered microphase-separated structure in the bulk, in which layers formed by the dense stacking of planarized polymer backbones are separated by more disordered side chain layers. This structure enables good transport of charges along the polymers (intrachain transport) as well as between polymer chains within the main chain layers.

It was also reported that the charge carrier mobility of regioregular P3HT depended significantly on the way how the films were prepared,[3−5] the kind of pretreatment of the dielectric gate insulator,[4,6−8] or the solvent used for film deposition.[3,9,10] Also, a strong dependence of the molecular weight on the charge transport properties of P3HT was found.[5,11,12] For example, Bao et al. and later Sirringhaus et al. pointed out that thin films of highly regioregular P3HT self-orient into a well-ordered lamellar structure with an edge-on orientation of the thiophene rings relative to the substrate ($\pi-\pi$ stacking direction parallel to the substrate).[3,4] Layers prepared from drop-cast and spin-cast films of highly regioregular (96% head-to-tail linkage) P3HT exhibited similar mobilities approaching 10^{-1} cm^2 V^{-1} s^{-1}. In contrast to that, spin-coated films of PHT with low regioregularity (81% head-to-tail linkage) consisted of lamellae with a face-on orientation, giving rise to low mobilities of ca. 10^{-4} cm^2 V^{-1} s^{-1} whereas the drop-cast films showed much higher mobility of ca. 4×10^{-3} cm^2 V^{-1} s^{-1}.[4]

More recently, Sirringhaus and co-workers reported a pronounced effect of the solvent from which the P3HT layers were spin-coated on the OFET properties.[9] By controlling the microstructure through the choice of the solvent while keeping the molecular weight of P3HT fixed ($M_w = 37\,000$ g/mol, *RR* $\approx$ 98%), they established a clear correlation between the field-effect mobility and the degree of microcrystalline order as measured by X-ray diffraction. This order manifested itself by

[†] University of Potsdam.
[‡] Institute of Ion Beam Physics and Materials Research.
[⊥] Fraunhofer Institute for Applied Polymer Research.
[||] University of Wuppertal.
[§] Max Planck Institute for Polymer Research.
[ϕ] New address: Leibniz Institute of Polymer Research, Hohe Strasse 6, D-01069 Dresden, Germany.
[#] New address: Institute of Physics, University of Siegen, Walter Flex Strasse 3, D-57068 Siegen, Germany.
* To whom correspondence should be addressed: e-mail neher@rz.uni-potsdam.de.

10.1021/ma0521349 CCC: $33.50
Published on Web 02/16/2006

the appearance of narrow higher order (*h*00) Bragg peaks (suggesting a regular stacking of the layers in the microphase-separated structure) and well-resolved (0l0) diffractions, indicating a well-ordered packing of the conjugated backbones in the main chain layers. The highest mobility was found in the films prepared from high boiling solvents, while rapid evaporation of low boiling solvents drastically reduced the time during which a well-ordered structure could be formed. Bao et al. also reported that the field-effect mobility of regioregular P3HT with a molecular weight $M_n = 11\,400$ g/mol strongly depended on the boiling point of the solvent and its solubility parameter. They proposed that the low charge carrier mobility in P3HT layers prepared from toluene and CH_2Cl_2 solvents was due to a particular morphology with distinct spherulitic grain boundaries (short nanorod-like fibrils). On the contrary, highly interconnected nanofibrillar networks formed in layers prepared from chloroform served as charge transport conduits without distinct grain boundaries, leading to high mobilities.[10]

McGehee et al. and we reported independently that the mobility of field-effect transistors made from P3HT increases strongly with increasing molecular weight.[5,11,12] In our investigations, raising the M_n of highly regioregular P3HT from 2200 to 19 000 g/mol resulted in field effect mobilities increasing from 5.5×10^{-7} to 2.6×10^{-3} $cm^2\ V^{-1}\ s^{-1}$.[12] Both groups reported consistently that layers of the low-M_n P3HT "appeared" more crystalline: crystalline grains could be identified by AFM experiments on thin layers of this fraction while X-ray reflection and grazing-incidence measurements provided clear evidence for a very high degree of order of the polymer chains in these grains. On the basis of these results, McGehee and co-workers suggested that the low mobility of the low-M_n fraction is due to trapping of charges at the boundaries of crystalline grains. In contrast, layers of the high-M_n fractions "looked" rather disordered, and no individual grains could be identified. This led to the suggestion that these layers consist of small ordered domains interconnected by long polymer chains. In fact, studies by McGehee et al. on layers deposited from different solvents supported the findings by Sirringhaus et al.[9] For a fixed molecular weight, solvents with high boiling temperature led to layers with well-resolved (0l0) diffraction signals and relatively high mobilities. On the other hand, the mobility of layers spin-coated from the low-M_n fraction remained significantly lower than those prepared from the high-M_n P3HT for all solvents tested. This supported the hypothesis that transport of charges within the microcrystalline grains must be rapid and that the significant effect of molecular weight on the charge carrier mobility is due to the presence of grain boundaries.

However, layers of the different fractions differed not only by their structural properties but also by their optical appearance. As discussed in detail in our previous paper,[12] the high-M_n fraction exhibits a well-structured solid-state absorption, with the maximum at 550 nm, while the low-M_n fraction shows a broad unstructured absorption peak centered at ca. 450 nm. Moreover, the solid-state absorbance of the low-M_n P3HT differs only little from that in solution. It is well-known that P3HT adopts a twisted conformation in solution, resulting in a short conjugation length and a blue-shifted absorption. The fact that the solid-state absorption of the short chain P3HT was quite comparable to its absorption in solution led us to the conclusion that the optical and transport properties of the low-M_n layers are mainly determined by a disordered matrix built from twisted chains, embedding highly ordered domains.

In this report, we present results of detailed investigations on powders and thin films of deuterated poly(3-hexylthiophene) (P3dHT) fractions with different molecular weights. The results strongly support our model that for the short chain P3HT the sample consists mainly of disordered domains, embedding thin crystallites of highly ordered chains. In contrast to this, for the long chain fractions, a larger number of chains are organized in crystalline or at least partially ordered domains, allowing charges to move parallel to the layer plane via various percolation pathways.

II. Experimental Section

For the investigations, deuterated regioregular poly(3-hexylthiophene) (P3dHT) was prepared by the Grignard metathesis procedure according to McCullough and co-workers.[13] Deuteration of side chains was chosen in order to perform neutron scattering experiments which are subject of further investigations. The raw polymer was fractionated by applying the so-called solvent extraction method.[14] Subsequent extraction steps with solvents of increasing solubility for P3dHT (ethyl acetate, hexane, dichloromethane, chloroform) yielded four polymer fractions with polydispersity index between 1.3 and 1.4. The average molecular weights were determined by using gel permeation chromatography (GPC) with THF as the solvent (calibration with narrowly distributed polystyrene standards). Powders of all P3dHT fractions have been precipitated from solvents into nonsolvents. Such powders are often highly crystalline.

Differential scanning calorimetry (DSC) thermograms were measured using a NETZSCH thermoanalyser 204. The measurements were carried out under a nitrogen atmosphere with heating and cooling rates of 10 °C/min. DSCs were taken from both powders and solution-crystallized samples. The latter were prepared from highly concentrated chloroform solution (50 mg/mL), which was added directly into the DSC pans. Then, the solvents were allowed to evaporate slowly. Using this procedure, homogeneous films were formed in the pan. Thereafter, these samples were soft-baked subsequently at 55 °C for 10 min, at 60 °C for 5 min, and finally at 65 °C for 15 min to remove residual solvent. Multiple heating and cooling cycles started with a heating scan from below room temperature (−50 or 0 °C where appropriate) and a rate of 10 °C/min. Melting and crystallization temperatures were determined by taking the peak values of the second heating and cooling scans, respectively.

X-ray diffraction (XRD) studies were performed to address the structural properties of powder and thin film samples of the P3dHT fractions. For XRD measurements of the P3dHT powders, a conventional powder diffractometer (D50000, Siemens) with a parallel incident beam and secondary graphite monochromator in front of the scintillation counter was used. The P3dHT powder was placed on a slowly rotating glass holder. For background correction, the scattering from the holder was subtracted. All samples were measured in reflection geometry using symmetrical $\theta/2\theta$ scans. The depth-resolved X-ray diffraction of the P3dHT thin films was carried out in noncoplanar grazing-incidence geometry (GID) at the beamline ID1 at the European Synchrotron Radiation Facility (ESRF) in Grenoble, France. By tuning the angle of incidence with respect to the sample surface, below or above the critical angle of total reflection, α_c, the penetration depth of the X-ray beam into the sample was controlled. Using this geometry, only diffraction signals from lattice planes that lay perpendicular to the sample surface were measured.

For transmission electron microscopy (TEM) examination, the spin-coated P3dHT thin films were removed from the silicon support by applying a drop of poly(acrylic acid) (PAA) onto the thin film. After hardening of the PAA, it was pealed off from the silicon support with the P3dHT thin film firmly adhering to the PAA. Subsequently, the PAA was dissolved in water, leaving the P3dHT film to float on the water surface. After careful rinsing with distilled water the film was transferred to a carbon-supported TEM grid. TEM examination was carried out using a LEO 912 operated at an acceleration voltage of 120 kV. Special care was taken to

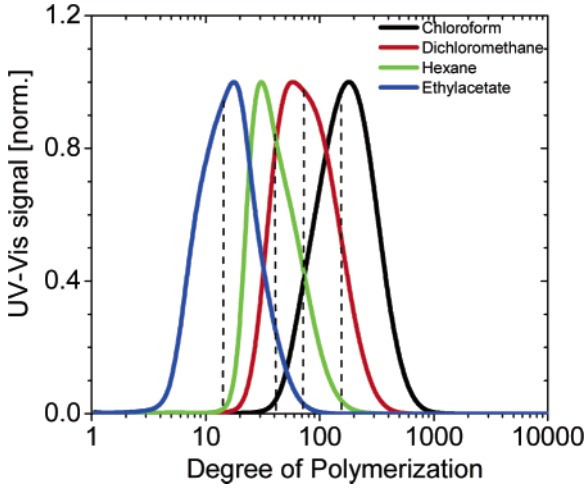

Figure 1. GPC diagrams of the four fractions obtained by selective extraction of regioregular P3dHT.

Table 1. Molecular Weight of the Studied P3dHT Fractions As Determined from GPC[a]

P3dHT fractions	M_n [g/mol]	M_w [g/mol]	PD	DP	L [nm]
chloroform	27051	35788	1.32	151	64
dichloromethane	12728	17161	1.35	71	30
hexane	7196	9203	1.28	40	17
ethyl acetate	2582	3623	1.40	14	5.9

[a] M_n = number-average molecular weight; M_w = weight-average molecular weight; PD = polydispersity; DP = the degree of polymerization as calculated from M_n; L = the length of one polymer chain calculated from DP.

minimize the irradiation damage to the sample by conducting the TEM examinations at a temperature of −120 °C.

III. Results and Discussion

Structure and Crystallization of Powder Samples. *GPC Studies*. Figure 1 shows the GPC diagrams of different fractions of regioregular P3dHT. Macromolecular parameters derived from the GPC diagrams are collected in Table 1. All fractions possess a rather broad molecular weight distribution with polydispersity index between 1.3 and 1.4. The average degree of polymerization of these fractions calculated from the number-average molecular weight M_n is between 14 for ethyl acetate fraction and 151 for chloroform fraction, corresponding to average chain lengths of 5.9 and 64 nm, respectively. Note that though the absolute M_ns of the different fractions differ significantly, there is significant overlap of the molecular weight distributions. In particular, the low-M_n fraction extracted with ethyl acetate exhibits a considerable number of chains with DP less than 10 (see Figure 1).

X-ray Studies. XRD data were measured on powders from all P3dHT fractions (see Figure 2).The scattering pattern of the ethyl acetate fraction has at least 11 sharp reflections and, thus, differs considerably from the scattering patterns of the three other fractions that exhibit only three broad peaks (see Figure 2). In this, our data are consistent with the previous XRD measurements on thin P3HT layers,[5,11,12] which also show that with the decrease in molecular weight the diffraction peaks become significantly sharper and that higher order diffraction peaks appear in the low molecular weight fraction.

In the present study, the higher molecular weight fractions show a broad (100) reflection peak corresponding to the chain−chain interlayer distance as well as the reflection peak at an angle of $2\theta = 23.4°$ caused by the stacking of the chains within the main chain layers. This latter peak is normally denominated

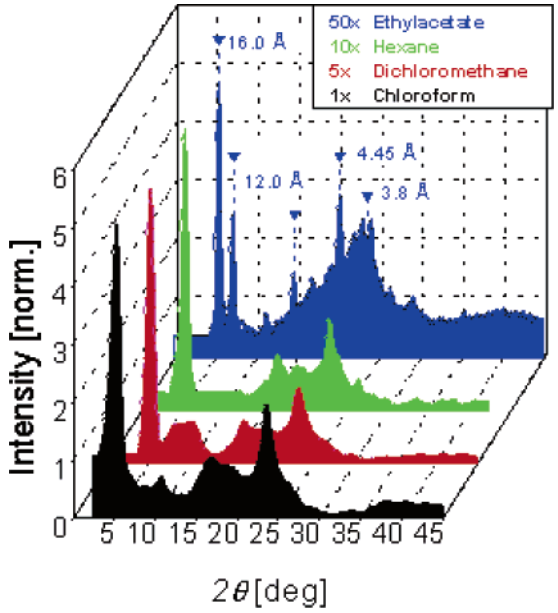

Figure 2. X-ray diffraction patterns of as-prepared P3dHT powders. The measured intensity is multiplied by the factor given in the legend. The ethyl actetate fraction revealed the lowest diffraction intensities but shows at least 11 sharp reflections and even higher order reflections (16 and 12 Å peaks).

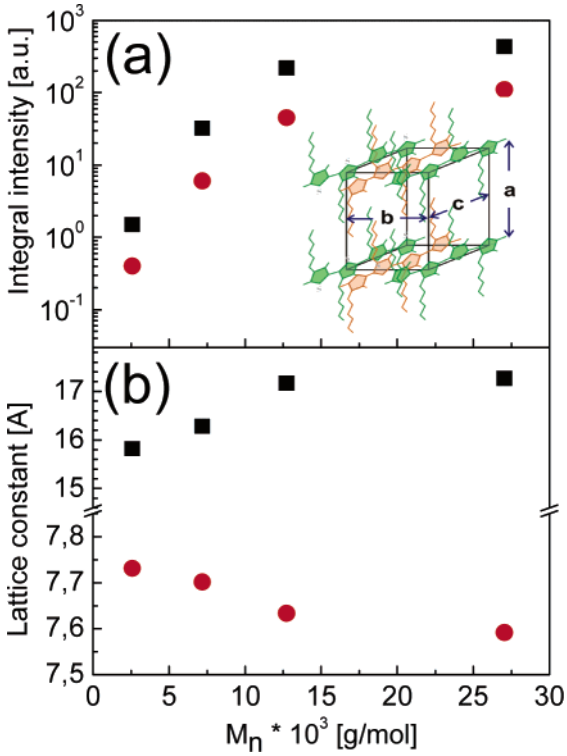

Figure 3. Integral intensities (a) and lattice plane distances (b) for the lattice constant a (■) and b (●) as a function of M_n, which were extracted from the XRD patterns shown in Figure 2. The insert picture in (a) shows the proposed unit cell by Winokur et al.[15]

as the (020) reflection. Interestingly, comparing the integral intensities of the two main peaks (100, 020), we found a steep increase with increasing molecular weight. The integral intensity for the chloroform fraction is about 400 times larger than that for the ethyl acetate fraction (see Figure 3a). On the other hand, the estimated crystallite size for ethyl acetate fraction is at least 4−5 times larger (more than 25 nm, a better estimation is restricted by the resolution function of the powder diffractometer) than that for chloroform fraction (see Table 2). Therefore,

Table 2. Degree of Crystallinity, ϕ_C, As Obtained from the Melting Enthalpies in the Second DSC Heating Runs on Powder Samples with Eq 3 and the Crystallites Size, *d*, Calculated from the Reflections at $2\theta = 5°$ and 24° (for the Ethyl Acetate Fraction, Peaks at 7° and 20° Were Used in Addition) in the XRD Measurements on Powder Samples of All P3dHT Fractions (Figure 2); Also Listed Are the Field-Effect Mobility μ_{OFET} Measured in the OFET Devices

P3dHT fractions	ϕ_C [%]	d [nm]	μ_{OFET} [$cm^2 V^{-1} s^{-1}$]
chloroform	18.0	7	7.4×10^{-3}
dichloromethane	16.0	5−7	4.0×10^{-3}
hexane	12.0	10	2.1×10^{-4}
ethyl acetate	4.5	>25	8.0×10^{-7}

we can assume that the number of chains organized in well-ordered domains increases largely with increasing molecular weight; however, the size and perfection of the crystallites decrease. The corresponding lattice constants (d_{100}, d_{020}) change as well with the molecular weight (see Figure 3b). If we consider the unit cell proposed by Winokur et al.,[15] then the chain−chain interlayer distance, $a \equiv d_{100}$, is found to increase from 15.8 Å for the ethyl acetate fraction to 17.3 Å for the chloroform fraction, while the chain−chain intralayer stacking distance, $b \equiv 2 \times d_{020}$, slightly decreases from ca. 7.8 to 7.6 Å with increase in M_n.

In addition to these two lattice planes, the scattering pattern of the ethyl acetate powder contains a series of sharp peaks corresponding to a lattice plane distance of 12.0 Å. Presently, we cannot distinguish whether the unit cell of the ethyl acetate fraction differs from that proposed by Winokur et al.[15] or whether there is a coexistence of two unit cells in the powder sample. The latter assumption is supported by studies on the morphology of regioregular poly(3-octylthiophene) (P3OT)[16] and poly(3-decylthiophene) (P3DT)[17] of different molecular weight. These studies showed consistently that the X-ray diffraction pattern of low molecular weight fractions exhibit additional peaks, which was attributed to a second polymorph (form II) with smaller interlayer spacing. For low molecular weight P3DT, these additional diffraction signals led to a unit cell assuming the second polymorph of $a = 17.0$ Å, $b = 5.08$ Å, $c = 7.76$ Å, and $\alpha = 95.0°$ ($Z = 2$), exhibiting a significantly smaller interlayer spacing and a larger intralayer stacking distance than for the more common form I ($a = 23.0$ Å, $b = 7.68$ Å, $c = 7.76$ Å, $\alpha = 93.2.°$; $Z = 4$).[17] Further, by comparing the results obtained for several P3ATs, with the number of carbon atoms in the side chains n between 4 and 16, a strictly linear dependence of the interlayer spacing with n was demonstrated, with $d = 12$ Å for P3HT. This is consistent with the lattice plane spacing mentioned above for the low-M_n P3dHT powder sample. Furthermore, the strong diffraction signal at 20.35° (corresponding to $d = 4.37$ Å) might be related to the intralayer stacking spacing in form II. The coexistence of two phases might also explain the presence of a broad melting transition in the DSC curves of the ethyl acetate fraction as discussed in the following.

Thermal Properties. Figure 4a−d shows the thermograms from solution-crystallized samples prepared from the chloroform, dichloromethane, hexane, and ethyl acetate fractions. The first heating cycle of the high molecular weight (chloroform) fraction exhibits a single narrow endothermic peak at 239 °C with a high melting enthalpy of 23.7 J/g. Upon cooling, a single exotherm is observed at 201 °C. The second heating scan exhibits, again, only one endotherm, though at slightly lower temperature (232 °C) and with a slightly smaller melting enthalpy ($\Delta H_{m,2} = 19.3$ J/g) as in the first heating run. Finally, as expected, the second cooling scan is identical to the first cooling cycle. In contrast to this, the first heating cycle of the ethyl acetate fraction shows two rather complex endotherms: one between ca. 30 and 63 °C and a second from 65 to 105 °C. This observation is in support of the proposed existence of two polymorphs in samples of this low molecular weight fraction. The total melting enthalpy, extracted from the area of both endotherms, is 4.5 J/g, much smaller than the value deduced for the high-M_n chloroform fraction. Upon cooling, a single

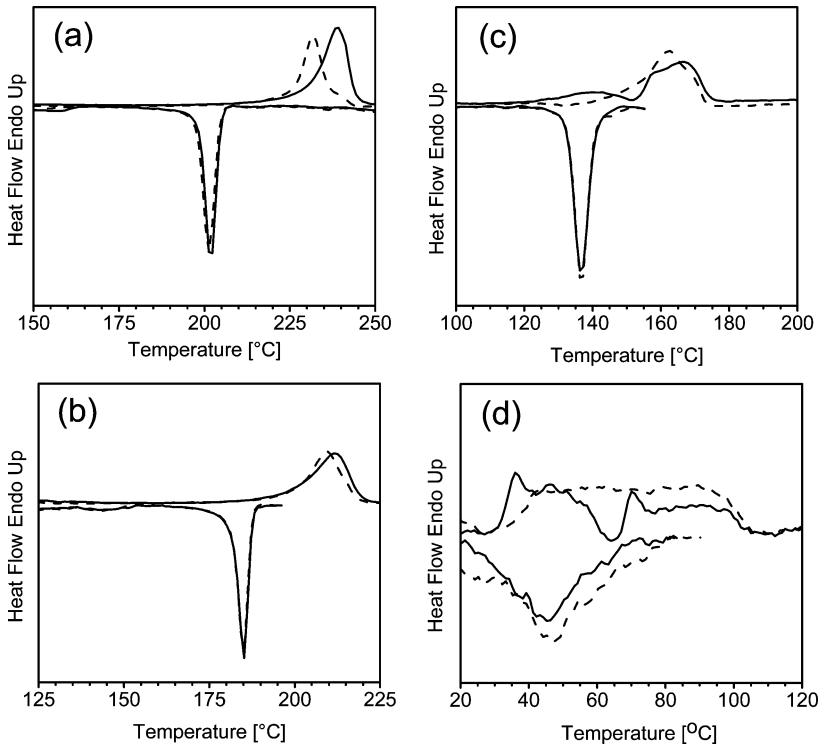

Figure 4. DSC thermograms measured from solution-crystallized samples of the chloroform (a), dichloromethane (b), hexane (c), and ethyl acetate (d) fractions. The solid and dashed lines refer to the first and second heating/cooling cycles, respectively.

Table 3. Melting Temperature (T_m), Crystallization Temperature (T_c), and Melting Enthalpy (ΔH_m) Measured from Solution-Crystallized Samples of All P3dHT Fractions (Figure 4)[a]

P3dHT fractions	$T_{m,1}$ [°C]	$T_{m,2}$ [°C]	$T_{c,1}$ [°C]	$T_{c,2}$ [°C]	$\Delta H_{m,1}$ [J/g]	$\Delta H_{m,2}$ [J/g]
chloroform	239.0	231.9	201.8	201.4	23.65	19.33
dichloromethane	211.9	209.2	185.1	185.1	17.71	15.99
hexane	166.0	162.7	136.7	136.7	12.02	12.01
ethyl acetate	36/70	70	46.3	47.3	4.54	5.75

[a] The subscripts 1 and 2 refer to the first and second heating/cooling cycles, respectively.

unstructured exotherm with the maximum at ca. 46 °C is observed. In the second heating run, a very broad single endotherm can be observed, covering the temperature range of both endotherms in the first heating scan and with similar total melting enthalpy ($\Delta H_{m,2} = 5.8$ J/g). The shapes and positions of the endotherms and exotherms in the DSC runs of the fractions of intermediate molecular weight lie somehow in between these two extremes. With decreasing molecular weight, the endotherms in the first heating cycle become more complex, the melting and crystallization temperatures decrease, and the melting enthalpies drop consistently. Melting and crystallization temperatures as well as melting enthalpies determined from the first and second heating DSC runs on the solution-crystallized samples are listed in Table 3.

At this point we note that the melting temperatures and enthalpies of the endotherms in the second heating run, which were performed immediately after the first cooling run, differ only little from those determined for the pristine samples (first heating run). This shows that the thermal properties of all fractions are only weakly affected by the history of the samples, which is crystallization from solution in the case of the pristine sample in the first heating run and crystallization from the melt or mesophase (during the first cooling) in the second heating. As expected, the DSC thermograms of solution-crystallized and powder samples were identical and fully reproducible except for the first heating run.

Both the melting and the crystallization temperatures increase almost linearly up to $M_n \sim 15\,000$ g/mol and then tend to saturate (see Figure 5a). The depression of the melting point with decreasing molecular weight is very pronounced: the melting point decreases by almost 150 K when reducing the DP from 71 to 14. In fact, the data predict that P3dHT with number-average molecular weights below 2000 g/mol should be rubbery at room temperature, and indeed, this was experimentally observed for a fraction with $M_n = 1500$ g/mol.

Several factors can be responsible for the observed depression of the melting point with decreasing molecular weight. It is known that since the chemical structure of the terminating monomer unit differs from that of the monomers along the chains, these terminal monomers constitute impurities. Therefore, the melting temperature and the molecular weight are related as follows:[18]

$$\frac{1}{T_m} - \frac{1}{T_m^0} = \frac{R}{\Delta H_m^0}\frac{2M_0}{M_n} \tag{1}$$

Here, T_m^0 is the melting temperature of a perfect crystal, R is the gas constant, ΔH_m^0 is the heat of fusion per mole of crystalline monomers, and M_0 is the molecular weight of the end monomer. If we define the average number of monomers in the chains of a particular fraction as $n = M_n/M_0$, then eq 1 can be rewritten in the following universal form:

$$\frac{1}{T_m} - \frac{1}{T_m^0} = \frac{R}{\Delta H_m^0}\frac{2}{n} \tag{2}$$

Equation 2 permits the calculation of both T_m^0 and ΔH_m^0 from the intercept and slope of a plot of $(1/T_m)$ vs $2/n$ (see Figure 5b). Interestingly, the data measured for the four P3dHT fractions lay nicely on a straight line, yielding $T_m^0 = 256$ °C and $\Delta H_m^0 = 1.07$ kJ/mol. Thus, the heat of fusion per gram of P3dHT is estimated to be about 6 J/g for $M_0 = 179$ g/mol. This value is considerably lower than that received from the DSC measurements described above (for example, the chloroform fraction has $\Delta H_m = 18$ J/g). Further, the melting temperature depression with decreasing chain length is much more pronounced than for conventional polymers. To illustrate this point, the solid line in Figure 5b shows the dependence of the melting point on the degree of polymerization for polyethylene (PE), calculated from eq 2 with theoretical values of T_m^0 and ΔH_m^0 from ref 18. Apparently, the melting temperature of P3dHT increases much steeper with the degree of polymerization. Thus, we conclude that the melting point depression in the P3dHT powders is not solely governed by the decrease of the average chain length but that the morphology of the solid material changes with molecular weight.

In addition, the analysis of the DSC thermograms according to

$$\phi_C = \frac{\Delta H_m}{\Delta H_m^0} \tag{3}$$

yields information on the crystallinity of the bulk samples. Here, ΔH_m is the heat of fusion for a particular fraction and ΔH_m^0 is the heat of fusion of an ideal (infinite and perfect) crystal. Values for ϕ_C have been calculated by dividing the melting enthalpies (Figure 6) obtained by integrating the melting peak in the second DSC heating runs of the powder samples by the value of $\Delta H_m^0 = 99$ J/g as taken from ref 19. According to the results summarized in Table 2, the chloroform fraction has the highest crystallinity of about 18%, while the ethyl acetate fraction has a very low crystallinity of about 4.5%. Note that the overall low degree of crystallinity of our samples agrees well with that reported for annealed regioregular P3HT crystallized from the melt.[19] For the ethyl acetate sample, the value of 4.5% gives the upper limit for the total fraction of chains crystallized in form I, since the specific melting enthalpy of form II is not known to us. Having in mind that samples with very short P3HT chains are rubbery at RT and that the molecular weight distributions of all fractions are considerably broad, we presume that only a small number of the chains with sufficient molecular length (from the high M_n part of the broad molecular weight distribution) forms crystallites by the stacking of fully extended chains, while the majority of chains are in a glassy or even rubbery state.

Structure and Crystallization of the Thin Films. The structure of thin films made from the low-M_n fraction was investigated using AFM, TEM, and XRD. Unfortunately, it was not possible to form layers from this fraction by drop-casting due to severe dewetting effects. Therefore, all studies were performed on ca. 50−90 nm thin spin-coated samples.

XRD Studies. Figure 7 shows the X-ray diffraction data at grazing-incidence and -exit geometry (XRD-GID) measured for the lowest (ethyl acetate) fraction and the highest molecular weight (chloroform) fraction. The data were measured by

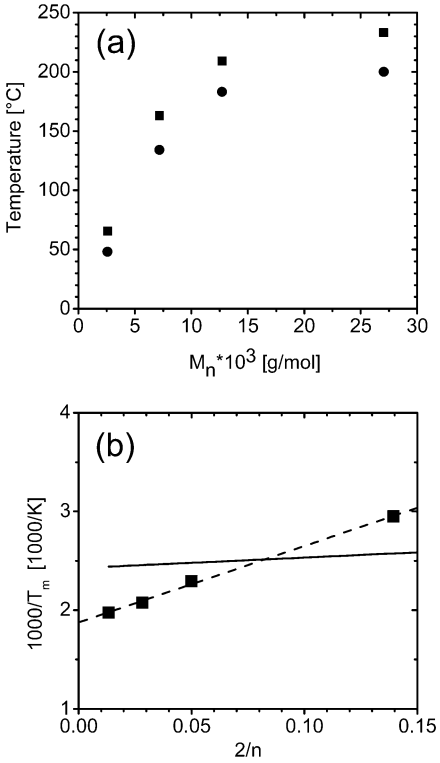

Figure 5. (a) Plot of the melting temperature T_m (■) and crystallization temperature T_c (●), taken from the second DSC heating and cooling runs on powder samples (see Figure S1), vs number-average molecular weight, M_n. (b) Plot of $1000/T_m$ vs $2/n$, where n is the average number of monomers in the chains of a particular fraction. The experimental data for the P3dHT fractions are indicated with (■), and the solid line shows the theoretical values for polyethylene (PE) taken from ref 18.

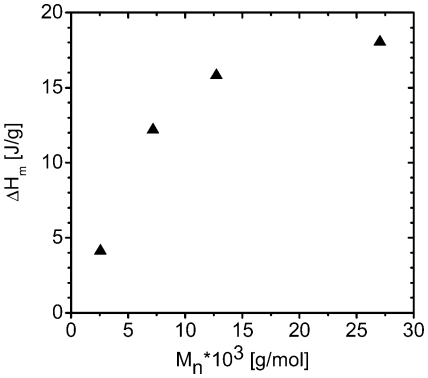

Figure 6. Melting enthalpies, ΔH_m, from the four P3dHT fractions measured by DSC on powder samples as a function of the number-average molecular weight, M_n.

scanning the in-plane detector angle $2\Theta_{in-plane}$ for fixed azimuth and fixed out-of-plane incidence angles $\alpha_i < \alpha_c$ and $\alpha_i > \alpha_c$, where $\alpha_c = 0.22°$ is the critical angle of total external reflection of the underlying silicon layer. When the incidence angle α_i is well below the critical angle of the substrate ($\alpha_i = 0.12°$ and $\alpha_i = 0.18°$), the X-ray wave penetrates only into the organic layer, and therefore, the scattering from the substrate in comparison to the thin film is suppressed. For an incidence angle of $\alpha_i = 0.12°$, the X-ray wave penetrates ~10 nm into the thin film; at a value of $\alpha_i = 0.18°$ the X-ray wave penetrates through the whole organic layer and the first few nanometers of the Si wafer. The influence from the substrate can be clearly seen at a larger penetration depth ($\alpha_i > \alpha_c$) where an increased scattering background at higher scattering angles can be recognized.

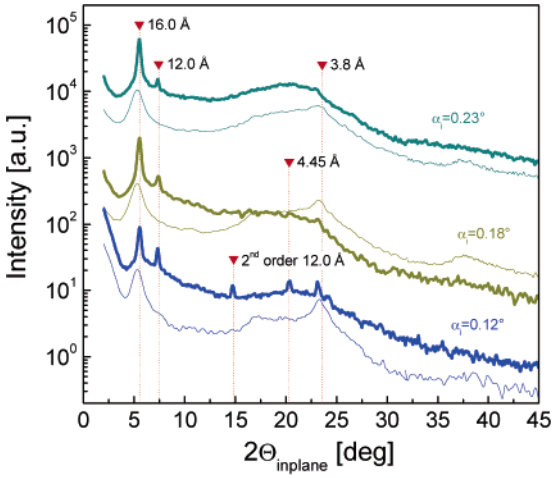

Figure 7. XRD-GID scans of thin layers prepared from the ethyl acetate and the chloroform P3dHT fraction, taken at different incidence angle in order to tune the penetration depth into the sample. Thick lines and thin lines show the results for the low- and high-M_n fraction, respectively.

There is a striking similarity of the X-ray diffraction pattern of the powder and the thin samples with regard to the position and width of the diffraction peaks. This indicates that, despite the very different methods of preparation, both types of samples exhibit similar morphologies. For the ethyl acetate fraction, the GID scan at $\alpha_i = 0.12°$ shows at least six reflection peaks, which appear at the same angular positions and have a similar intensity distribution like the powder diffraction data for the same fraction. Note that GID is only sensitive to order in the plane. Thus, the appearance of pronounced (100) reflections for both fractions indicates that the orientation of the main chain layers in the crystals is not exclusively parallel to the layer plane.

AFM and TEM Studies. We have reported earlier that the low-M_n fraction layer (as-prepared) exhibits whiskers (or ribbons) of 100−200 nm length. These whiskers can be clearly identified in the phase AFM image shown in Figure 8a. The apparent average width of these long whiskers is 25 ± 8 nm, corresponding to a real geometrical width of ~11 nm.[12] Since the length of one polymer chain in the low molecular weight fraction is ca. 6 nm on average, we conclude that the polymer backbones are oriented normal to the long axis of the whiskers. Further, a width of ca. 11 nm, larger than the average chain length, is in agreement with the interpretation drawn above that the whiskers are built from the longest chains in the molecular weight distribution, while the shorter chains form the disordered matrix.

Complementary TEM examinations corroborate the AFM results and reveal additional structural information. In the bright field (BF) micrograph (see Figure 8b) similar whiskerlike structures can be observed. Note that bright field images had to be taken with a certain amount of underfocus (phase contrast) in order to visualize the contrast of those whiskers, indicating that the thin P3HT films consist of two phases, a crystalline one which is embedded in an amorphous region. Contrary to that, if the whiskers are not embedded within a matrix, it would show a mass-thickness contrast in TEM, noticeable by in-focus visibility. Since this is not the case, the assumption of a two-phase system with crystals embedded in amorphous matrix is highly probable. Further, to identify the crystalline character of this fraction, we recorded the electron diffraction pattern as shown in Figure 8c. It shows a polycrystalline pattern with only one sharp ring corresponding to a lattice spacing of 3.6 Å. This value agrees well with the XRD value measured on powder

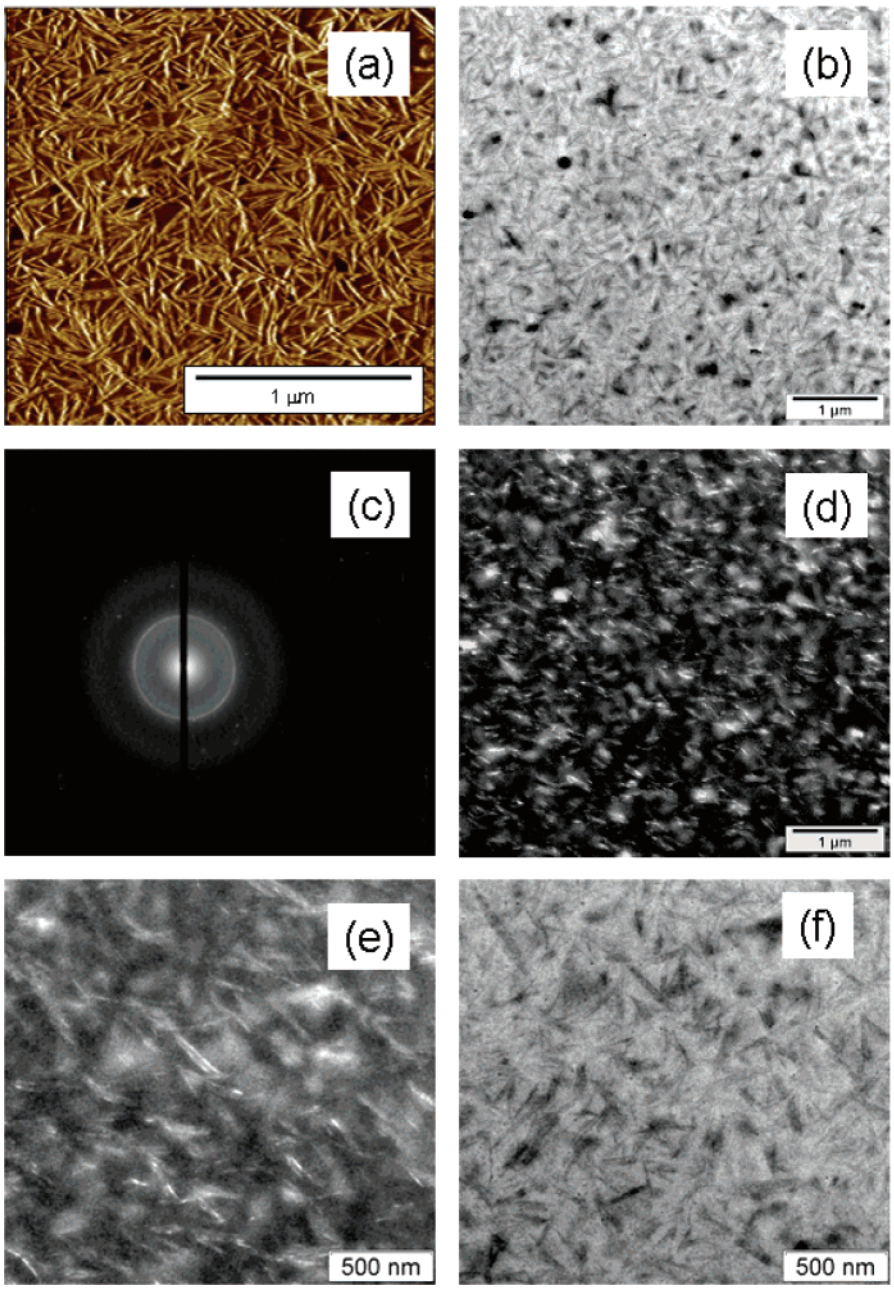

Figure 8. Structural properties of thin films prepared from the low-M_n fraction: (a) AFM phase image, (b) TEM bright field image, (c) TEM diffraction pattern, (d) TEM dark field image, (e) TEM dark field image with higher magnification, (f) TEM bright field image with higher magnification. The AFM image was taken at room temperature while TEM was performed at −120 °C to avoid damage of the layers due to the electron beam.

samples. To identify the crystalline component, dark field (DF) imaging using this reflection was performed. Figure 8d shows the DF micrograph corresponding to the BF image in Figure 8b. Several bright whiskerlike structures can be observed, indicating that they are crystalline. However, only a few of the whiskerlike structures visible in the BF can be found in the DF image. This is due to the special imaging conditions in DF mode that uses the objective aperture to select a certain arc from the diffraction ring. Only those electrons that pass this aperture will contribute to the final DF image. This means that only those crystallites that have a certain crystal orientation with respect to the microscope adjustment can be seen in the DF images. The multicrystalline morphology of the layer is clearly seen in the DF and BF micrographs recorded with higher magnification (Figure 8e,f). In fact, individual whiskers of a length of up to 500 nm and a width of 11 ± 2 nm can be resolved. These values are in full agreement from the findings from AFM imaging. The graphs also display nicely that many of the whiskers are bundled together and that these bundles are surrounded by a noncrystalline phase.

A closer inspection of the BF images suggests that the overall crystallinity of the thin layers of the lowest molecular weight fraction must be larger than the 5% deduced from the DSC measurements on bulk samples. (A graphical analysis of Figure 8f suggests a crystallinity of almost 30%.) This discrepancy might have several reasons. First, TEM images show only a 2D in-plane projection of the layers. Thus, TEM overestimates the crystallinity of the sample if the crystallites do not extend through the whole layers. Note that the GID spectra of the low molecular weight samples become considerably less structured with increasing incident angle (corresponding to an increasing penetration depth), which is only partially due to an increasing

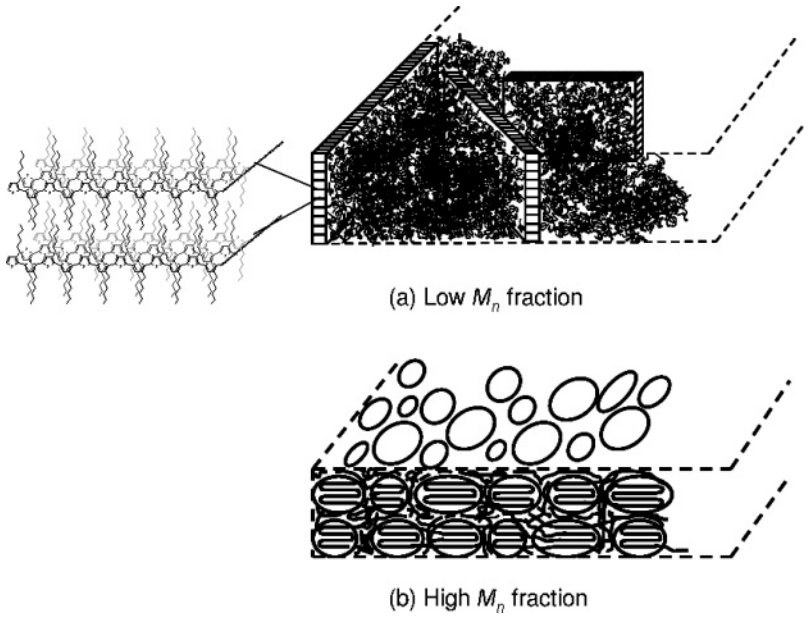

Figure 9. Schemes of the morphologies of thin layers of the low-M_n and high-M_n fractions. In these simplified pictures, the main chain layers in the ordered regions are assumed to be oriented exclusively parallel to the layer plane, with the side chains (not shown) extending perpendicular to the layer plane. For the ethyl acetate fraction, the crystallites extend throughout the whole layer thickness and consist of fully extended chains. These crystalline whiskers are embedded into a disordered matrix. Layers of the high-M_n chloroform fraction consist of small partially ordered domains, with the average width smaller than the chain length. Thus, chains either fold back, extend into the disordered phase, or interconnect neighboring domains.

influence of the "thin film−substrate" interface. These measurements indicate that though the crystallites are distributed over the whole film thickness, the crystallinity might be highest in a region close to the surface of the layer. Second, the XRD data of the low molecular weight fraction (powder and thin film) suggest the presence of a second form II with different lattice parameters. This polymorph might have a lower melting enthalpy than the common form I, and the overall crystallinity of the low molecular weight samples might thus be larger.

Strong evidence that only a small fraction of the chains in these layers is organized in lamellae with closely packed planarized backbones comes from optical absorption studies. As published earlier, the optical appearance of the thin P3HT films changes significantly with molecular weight.[12] Most important, the solid-state absorbance of the ethyl acetate fraction at RT almost resembles that of the corresponding solution (see Figure S2), with only little extinction in the wavelength range where domains of planarized polythiophene chains exhibit a well-structured absorption. Moreover, the characteristic changes in the solid-state absorption spectra with decreasing molecular weight quite resemble those measured for layers of high-M_n regioregular P3HT with a fixed molecular weight when increasing the temperature. This well-known thermochroism has been assigned to the melting of crystalline or partially ordered phases, accompanied by the thermally induced continuous transition from a planar rigid-rod backbone conformation at RT to a twisted coillike conformation above the melting point of the main chains. The fact that the absorption of the short chain P3HT at RT quite resembles that of the well-studied long chain P3HT close to the melting transition strongly supports our argument that the crystallinity of the layers formed from the low-M_n fraction must be low. Finally, we note that there is a pronounced blue shift of the absorption of these layers upon heating already when starting at RT (while there is no change in the shape of the absorption spectrum of high-M_n layers up to a temperature of more than 120 °C). Apparently, the low-M_n material is in the thermochromic region at RT, implying that only a small fraction of the chains exhibits a planarized backbone conformation while most chains are in the twisted (most likely disordered) state.

IV. Discussion and Conclusions

In the following we like to discuss the results summarized above with respect to the significant changes in the transport properties of P3HT solid layers when decreasing the chain length. Concerning the morphology of the solid state of the low-M_n P3HT fractions, the results reported here and published by others provide consistent proof that the powder samples as well as the thin layers exhibit crystallites with a width of ca. 10 nm and a length of several tens to hundreds of nanometers, consisting of regularly stacked chains. At the moment, we cannot provide a full interpretation of the X-ray diffraction scans, but the results indicate the coexistence of two difference polymorphs, which differ in the intralayer stacking distance and, possibly, in the orientation of the main chain layers with respect to the substrate.[17] On the other hand, the low melting enthalpy in the DSC of the bulk samples (Figure 6), the low diffraction intensities in the powder X-ray diffraction experiments, and, most conclusively, the results of the TEM experiments on the thin polymer layers leave little doubt that these crystalline regions represent only a minor fraction of the sample volume. Having in mind that very short P3HT chains are not able to crystallize at RT, it is plausible to assume that crystals of the longer chains in the molecular weight distribution of the ethyl acetate fraction are embedded within a disordered matrix consisting of the shorter chains, as illustrated in Figure 9a. In fact, such a viscous matrix would allow the chains in the crystals to arrange in a very regular and highly ordered fashion. The interpretation that the solid state of the low-M_n fraction consists mainly of disordered regions formed by twisted chains is further consistent with the observation reported earlier by us that the solid-state absorbance of this fraction differs only little from that in solution.[12]

The picture about the morphology of the high-M_n chloroform fraction is less complete. Indeed, no distinct features could be resolved in the TEM images of thin layers of the high-M_n

fraction. While the rather large melting enthalpy as well as the large intensity of powder X-ray diffraction peaks indicate that a large fraction of the chains is within ordered domains, the rather large width of the diffraction peaks and the almost complete absence of higher order diffraction signals indicates that the degree of order of the chains in these domains is not very high. Following the arguments given in ref 20, we propose that our samples consist of crystalline, partially ordered, and disordered phases. (The coexistence of at least three phases in high-M_n P3HT has been proposed in order to explain the rather continuous shift of the solid-state absorption of regioregular P3HT with increasing temperature.) We also like to point out that the average length of the polymer chains in the chloroform fractions probably exceeds the size of ordered domains as extracted from the XRD experiments. High-M_n regioregular P3HT was reported to crystallize in a chain-folded fashion under certain conditions, forming ca. 15 nm wide whiskers, with the P3HT chains oriented mainly perpendicular to the growth direction of the whiskers.[19−21] Thus, the ordered domains in our high-M_n P3HT samples might include back-folds and could as well be interconnected by long chains (Figure 9b).

These structural models can be used to explain consistently the transport characteristics of the layers made from the different fractions. In the FET geometry, transport is exclusively parallel to the layer plane. Presuming that the mobility in the disordered phase is very low, charges need to travel via a percolation-type motion through the ordered domains. As shown by the TEM pictures (see Figure 8), most of the crystalline domains in the low-M_n layers are isolated by the amorphous matrix, and transport will be mainly between the few interconnected domains. In contrast to this, because of the larger number of chains organized in ordered domains in the high-M_n layers, many pathways exist for the carriers to travel parallel to the layer plane. In fact, the large increase in mobility over 4 orders of magnitude in the OFET geometry (see Table 2) for an increase in crystallinity from ca. 5% to 20% (using the values measured for the powder samples) resembles the properties of percolation networks. This further suggests that the transport of charges parallel to the layer plane is mainly controlled by the crystallinity of the samples. Moreover, the differences in morphology as depicted in Figure 9 are consistent with the finding that the charge carrier mobility measured perpendicular to the layer plane varies less pronounced with molecular weight than for transport perpendicular to the layer.[22] In fact, a zero-field mobility of 1.3×10^{-5} cm^2 V^{-1} s^{-1} was reported for a short chain fraction with M_w of ca. 2890 g/mol compared to 3.3×10^{-4} cm^2 V^{-1} s^{-1} for a fraction with $M_w = 31\,100$ g/mol. Considering a coherence length >25 nm as deduced from the X-ray reflections scans of the short chain layers, it is meaningful to conclude that a large number of crystalline grains extend throughout the whole layer thickness, providing pathways for transport perpendicular to the layer plane.

Moreover, this picture is consistent with the reported temperature dependence of mobility parallel and perpendicular to the layer plane. For transport parallel to the layer, the main difference between the different fractions should be the number of percolation pathways from the source to the drain electrode. It was reported by McGehee et al. that for temperatures below RT the mobility follows an Arrhenius-type behavior and that the activation energy changes only slightly with molecular weight.[5] This implies that the temperature dependence of the mobility origins mainly from the temperature-activated transport (hopping transport) within the ordered domains. For transport perpendicular to the layer plane, the activation energies were larger (ca. 130 meV compared to ca. 60 meV for transport parallel to the plane) but changed only little with molecular weight. This is again consistent with our view that the transport within the grains is mainly relevant to the macroscopic current flow and that this transport is temperature-activated.

Finally, as we have reported previously, the in-plane mobility decreases considerably above RT for a low-M_n batch. This decrease goes in parallel with the pronounced thermochroism of the layer.[12] If we presume that transport is almost exclusively along interconnected ordered domains, the significant decrease of the mobility with temperature can be conclusively explained by the continuous reduction of the crystallinity of the samples when approaching the melting temperature.

In conclusion, our results give strong evidence that the transport properties of layers prepared from fractions of poly(3-hexylthiophene) with different molecular weight is largely determined by the crystallinity of the samples. We presume that this correlation is rather universal and, in part, responsible for the strong dependence of the OFET mobilities for polymer OFETs on the preparation conditions. Thus, previous reports on the effect of the regioregularity of the polymer and of the choice of the solvent used to coat the layers on the OFET properties need to be reconsidered again in view of this correlation.

Acknowledgment. We thank H. Metzger and D. Carbone for their valuable help at the ESRF beamline ID1. This work was financially supported by the German Science Foundation, the Fond der Chemischen Industrie, and the Ministerium für Wissenschaft, Forschung und Kultur of Brandenburg.

Supporting Information Available: DSC thermograms of powder samples of four P3dHT fractions (Figure S1) and absorption spectra of P3dHT (Figure S2). This material is available free of charge via the Internet at http://pubs.acs.org.

References and Notes

(1) Gamota, D. R., Brazis, P., Kalyanasundaram, K., Zhang, J., Eds. *Printed Organic and Molecular Electronics*; Kluwer Academic Publisher: Dordrecht, 2004.
(2) Assadi, A.; Svensson, C.; Willander, M.; Inganäs, O. *Appl. Phys. Lett.* **1988**, *53*, 195.
(3) Bao, Z.; Dodabalapur, A.; Lovinger, A. J. *Appl. Phys. Lett.* **1996**, *69*, 4108.
(4) Sirringhaus, H.; Brown, P. J.; Friend, R. H.; Nielsen, M. M.; Bechgaard, K.; Langeveld-Voss, B. M. W.; Spiering, A. J. H.; Janssen, R. A. J.; Meijer, E. W.; Herwig, P. T.; de Leeuw, D. M. *Nature (London)* **1999**, *401*, 685.
(5) Kline, R. J.; McGehee, M. D.; Kadnikova, E. N.; Liu, J.; Frechet, J. M. J.; Toney, M. F. *Macromolecules* **2005**, *38*, 3312.
(6) Merlo, J. A.; Frisbie, C. D. *J. Polym. Sci., Part B: Polym. Phys.* **2003**, *41*, 2674.
(7) Gorjanc, T. C.; Levesque, I.; Lorio, M. D. *Appl. Phys. Lett.* **2004**, *84*, 930.
(8) Zen, A.; Neher, D.; Silmy, K.; Holländer, A.; Asawapirom, U.; Scherf, U. *Jpn. J. Appl. Phys., Part 1* **2005**, *44*, 3721.
(9) Chang, J.; Sun, B.; Breiby, D. W.; Nielsen, M. M.; Solling, T. I.; Giles, M.; McCulloch, I.; Sirringhaus, H. *Chem. Mater.* **2004**, *16*, 4772.
(10) Yang, H.; Shin, T. J.; Yang, L.; Cho, K.; Ryu, C. Y.; Bao, Z. *Adv. Funct. Mater.* **2005**, *15*, 671.
(11) Kline, R. J.; McGehee, M. D.; Kdnikova, E. N.; Liu, J.; Frechet, J. M. J. *Adv. Mater.* **2003**, *15*, 1519.
(12) Zen, A.; Pflaum, J.; Hirschmann, S.; Zhuang, W.; Jaiser, F.; Asawapirom, U.; Rabe, J. P.; Scherf, U.; Neher, D. *Adv. Funct. Mater.* **2004**, *14*, 757.
(13) Loewe, R. S.; Khersonsky, S. M.; McCullough, R. D. *Adv. Mater.* **1999**, *11*, 250.
(14) Trznadel, M.; Pron, A.; Zagorska, M.; Chrzaszcz, R.; Pielichowski, J. *Macromolecules* **1998**, *31*, 5051.
(15) Prosa, T. J.; Winokur, M. J.; Moulton, J.; Smith, P.; Heeger, A. J. *Macromolecules* **1992**, *25*, 4364.

(16) Bolognesi, A.; Porzio, W.; Zhuo, G.; Ezquerra, T. *Eur. Polym. J.* **1996**, *32*, 1097.
(17) Meille, S. V.; Romita, V.; Caronna, T.; Lovinger, A. J.; Catellani, M.; Belobrzeckaja, L. *Macromolecules* **1997**, *30*, 7898.
(18) Sperling, L. H. *Introduction to Physical Polymer Science*, 3rd ed.; John Wiley & Sons: New York, 2001.
(19) Malik, S.; Nandi, A. K. *J. Polym. Sci., Part B: Polym. Phys.* **2002**, *40*, 2073.
(20) Yang, C.; Orfino, F. P.; Holdcroft, S. *Macromolecules* **1996**, *29*, 6510.
(21) Ihn, K. J.; Moulton, J.; Smith, P. *J. Polym. Sci., Polym. Phys.* **1993**, *31*, 735.
(22) Goh, C.; Kline, R. J.; McGehee, M. D.; Kadnikova, E. N.; Frechet, J. M. J. *Appl. Phys. Lett.* **2005**, art. no. 122110.

MA0521349